ORIGINAL

Experimental and numerical analysis of the pyrolysis dynamics of a single wood particle: presentation of the radiographic technique

Paweł Kazimierski[1] · Katarzyna Januszewicz[2] · Paulina Hercel[1] · Dariusz Kardaś[1]

Abstract

Pyrolysis is an oxygen-free process for the thermal decomposition of raw materials. The heat conduction and flow of pyrolysis products (i.e., the gas fraction and liquid vapour generated during pyrolysis) influence the process and products. In this work, the influence of the orientation of wooden particle fibres with respect to the direction of the heat source on the dynamics of the process was investigated, where there were two particle sizes oriented along or across the heat source. The novelty of this work lies in the use of a radiographic technique for analysing the influence of wooden fibres' orientation on the degradation process. The research showed that during pyrolysis, the mass loss rate in the particles with fibres oriented across the heat source and along the heat source was different. A similar tendency was characteristic for the drying process. The dynamics of pyrolysis of a single wood particle depends on many factors—particle size, process parameters, arrangement of fibres in wood, etc. The analysis of the dynamics presented in the publications is based on the analysis of the dynamics of mass loss, which is a very large simplification. The publication contains experimental analysis and mathematical calculations of the pyrolysis process for samples of various sizes and samples with different fibre arrangement. The result of the research is the determination of trends regarding the shape of the particle and the arrangement of fibres on the process, which provides knowledge that can be translated into industrial pyrolysis processes.

✉ Paweł Kazimierski
  pkazimierski@imp.gda.pl

  Paulina Hercel
  phercel@imp.gda.pl

  Dariusz Kardaś
  dk@imp.gda.pl

[1] Institute of Fluid Flow Machinery, Polish Academy of Sciences, Fiszera 14, 80-231 Gdańsk, Poland

[2] Department of Energy Conversion and Storage, Chemical Faculty, Gdańsk University of Technology, Narutowicza 11/12, 80-233 Gdańsk, Poland

Introduction

Nowadays, the amount of fossil fuels is limited, and efficient renewable energy sources are being sought after. One of the solutions is the use of biomass due to its advantage of being able to generate energy continuously, regardless of atmospheric conditions or the time of day. The pyrolysis process is considered one of the keyways to produce, among others, charcoal or biochar (Kazimierski et al. 2022).

To generally characterize the process of biomass decomposition, we can distinguish three main stages. The preliminary stage is drying, where an isothermal process takes place at a temperature below 150 °C at atmospheric pressure. Evaporation of water is not a chemical process like pyrolysis, gasification or combustion; however, it is a crucial preliminary stage during degradation. Lignocellulosic biomass, such as wood, is a heterogeneous material, and the structure and amount of water depend on various factors, e.g., the part of the plant (Yin et al. 2023), season, and species. Therefore, a particle with a high humidity (up to 50 wt. %) requires a long time to heat due to evaporation, and the energy absorbed by this process may disturb the subsequent gasification, combustion or pyrolysis processes. However, the time for complete vaporization of biomass depends on many factors, such as the shape and size of the material and supplied heat flux. Extensive descriptions of the drying process of a single fuel particle is described based on both experiments and numerical modelling (Wardach-Święcicka et al. 2013). The experimental work for the water evaporation from a single fuel particle proceeds differently than for a whole bed (Ronewicz 2017). In a case of single particle, the moisture 'moves' from the inside to the outside of the particle due to a decrease in the moisture in the outer parts. The described process of drying takes place during steam heating and motion of gasses around the particle. The second stage of pyrolysis is conversion, where the volatiles are released as a result of the beginning of hemicellulose decomposition (Kardaś et al. 2014a; 2014b). The least stable chemical bonds in the hydrocarbons break down at the beginning during the conversion stage. The shorter chains of hydrocarbons are formed and are released as volatile components (Demirbas et al. 2001). These compounds are reactive and undergo secondary reactions outside and inside the particle, as indicated by the various masses of volatile parts that depend on the size of the pyrolysed particle (Jesus et al. 2019). Finally, the third stage involves slow transformation. The physical properties of char (porosity, deformation in relation to the shape of the raw biomass, and density) depend on the conditions of its acquisition as well as the raw material used in the process (Kazimierski et al. 2021). The activation process at high temperatures that influences the carbon surface was investigated and is described elsewhere (Januszewicz et al. 2020).

Internal dynamics are crucial in the pyrolysis of solid fuels. One important mechanism is the volume shrinkage that occurs during char conversion. Failing to account for this can significantly impact predictions of char yield and pyrolysis rate. In addition, realistic microstructure models are also important for differentiating the intraparticle transport for various feedstocks. However, there have

been limited amounts of experiments that report detailed measurements of these internal dynamics due to challenges such as limitations in optical access and high spatial and temporal resolution requirements. Radiographic (X-ray image analysis) testing is one of the research techniques that has been previously used to measure permeability and image pyrolysis formation in biomass (Boigne et al. 2022; Jones et. al. 2015; Kazimierski et al. 2020; Haboub et al. 2014). In another study, the focus was on the pyrolysis process from the perspective of wood biomass, utilizing high-speed X-ray computer tomography (CT) for the investigation (Murai et al. 2021). The CT can produce high-resolution images with fine details, making possible to detect small defects or changes in material properties (Boigne et al. 2021). In addition, CT can be used to perform in situ measurements of the pyrolysis process, allowing researchers to study the process under real-world conditions (Boigne et al. 2022). On the other hand, after reviewing the literature, it was noticed that there are few articles that describe the results of studies using X-ray analysis techniques to observe the pyrolysis process. (Mathews et al. 2017; Barr et al. 2021). To complement the existing results, it was decided to use this technique to observe the effect of the pyrolysis process on the sample, taking into account its structure. In this work, the authors showed the potential of using X-ray image analysis to capture internal thermal degradation dynamics in dense and optically inaccessible wood samples. X-ray image analysis is typically a more cost-effective method compared to high-speed X-ray CT, which requires specialized equipment and can be more expensive to perform. X-ray image analysis has been shown to be effective in capturing internal thermal degradation dynamics in dense and optically inaccessible wood samples, which is important for understanding the pyrolysis process. The advantage of CT is the ability to perform 3D measurements as opposed to 2D radiography, although CT requires a more complex and longer acquisition process.

The novelty of this work is the use of this research technique in evaluating the kinetics of the pyrolysis process and the effect of the fibre arrangement of wood samples on the obtained char. The orientation of wood fibres has an important influence on the drying and pyrolysis process (Suleiman et al. 1999). In the homogeneous structure of a particle, the moisture distribution during drying is predictable and increases towards the centre of the particle. The complicated structure of the wood and arrangement of fibres along and across the particle cause different vaporization process rates. The dependencies of the rate of removing water on the structure of wood have been described by Ronewicz (2017) and Kluska et al. (2019). In both works, the evaporation as a function of the orientation of the fibres with respect to the heat source was investigated. Ronewicz (2017) performed an experimental study using wooden cubical samples dried with a stream of hot air. He obtained lower final masses for samples with fibres oriented in the same direction as the air flow than for samples with fibres oriented perpendicular to the air stream. The evaporation of water reflects the degassing process of volatile components as well since both water and volatiles leave the particle through the same elements of the wood structure. The thermal conductivity coefficient for wood varies from 0.17 to 0.56 W/(m K) (Guo et al. 2013), and these values are much lower than those for steel or ceramics. The fluctuation of the thermal

conductivity of wood results from its internal, anisotropic structure. Open channels in the wood structure are filled with air that provides a high thermal insulation and influences the resultant heat conductivity of the sample (Kollmann et al. 1968; Siau 1984; Forest Service 2020 F2).

The aim of this study is to investigate the internal dynamics of biomass combustion and provide detailed experimental measurements using radiographic testing (X-ray image analysis). The study has three main objectives. Firstly, it aims to provide fundamental insights and reference data by examining the volume shrinkage and reaction fronts of pyrolysis and oxidation inside the fuel for different arrangement of the fibres of the wood sample. Secondly, the study investigates the impact of structure on kinetic parameters of pyrolysis process. Lastly, the study aims to advance the capabilities of X-ray image analysis as a method for providing reference measurements and guiding the development of heterogeneous pyrolysis models and the obtained results can be used in the construction of technological solutions on an industrial scale. The permeability of gas and steam in wood is an important parameter that influences the pyrolysis process. Two types of flow can be observed in a wood sample during pyrolysis: axial (along the fibres) and radial (across the fibres). Axial flow contributes much more to the discharge of pyrolysis volatile products during the process.

Materials and methods

Sample preparation

Two sample sizes and two wooden fibre orientations (along and across the heat source) in beech wood *(Fagus sylvatica)* samples were used in this investigation. The cuboid samples had dimensions of $20 \times 20 \times 5$ mm and the cubic samples had dimensions of $32 \times 30 \times 30$ mm. The cubic samples were insulated with foam rubber (for drying) or vermiculite (for pyrolysis). In this case, only one wall with wooden fibres along or across the heat source was subjected directly to the provided heat. The influence of the orientation of the fibres with respect to the heat source on the pyrolysis process was investigated (Figs. 1 and 2). The following abbreviations for the sample types are used in this manuscript:

- AC—non-insulated sample with dimensions of $20 \times 20 \times 5$ mm, where the fibres were oriented across the heat source
- AL—non-insulated sample with dimensions of $20 \times 20 \times 5$ mm, where the fibres were oriented along the heat source
- IAC—insulated sample with dimensions of $32 \times 30 \times 30$ mm, where the fibres were oriented across the heat source
- IAL—insulated sample with dimensions of $32 \times 30 \times 30$ mm, where the fibres were oriented along the heat source.
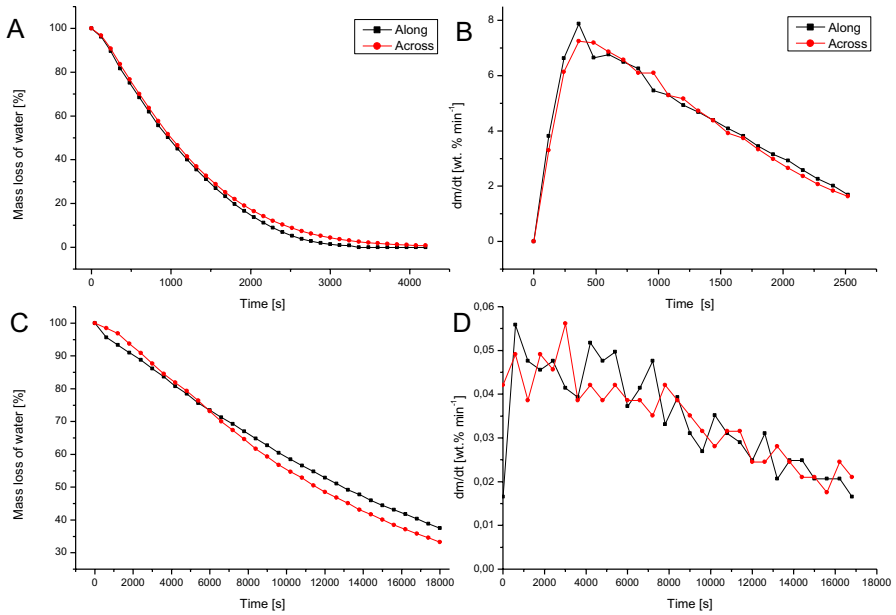
Fig. 1 Experimental data of drying process dynamics for particles with fibres oriented across and along the heat source: **A** and **B** AC and AL samples with a size of $20 \times 20 \times 5$ mm (not insulated) and **C** and **D** IAC and IAL samples with a size of $32 \times 30 \times 30$ mm (insulated on 5 walls)
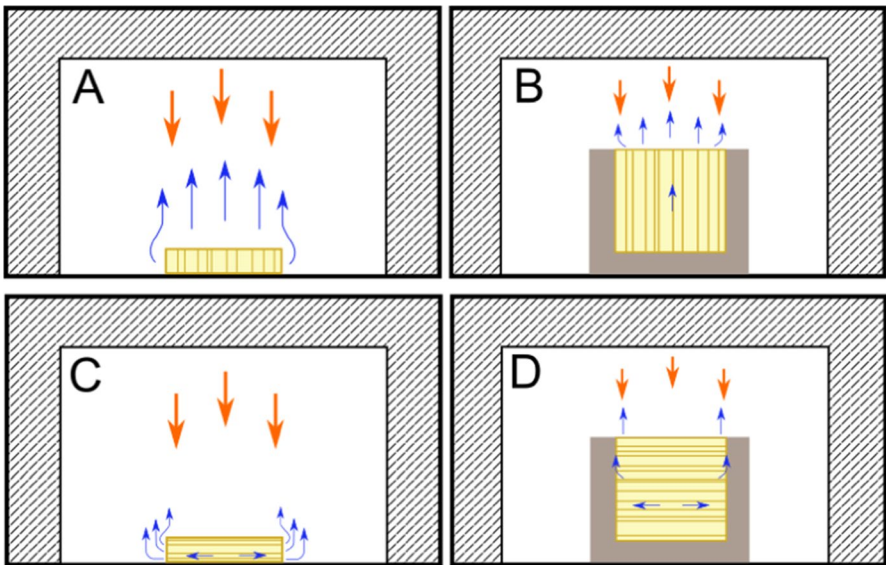
Fig. 2 Heat and flow distributions during the drying process for samples with fibres oriented across the heat source: **A**. AC and **B**. IAC. Heat and flow distributions for samples oriented along the heat source: **C**. AL and **D**. IAL (arrows pointing from top to bottom- heat distribution; arrows pointing from bottom to top- steam)

Drying process

The drying process was conducted in the laboratory using a dryer and moisture analyser (dryer, moisture analyser RADWAG MAX 50/NH).

The samples (IAC and IAL) with a size of 32×30×30 mm were insulated on 5 sides only, and one side of the sample was submitted to the high temperature. All samples were dried in the moisture analyser at 105 °C for 24 h, and the samples were weighed. In the next part of the experiment, the samples were moisturized with water again to the level of 50%. Samples prepared in this way were subjected to experiments. During the drying analysis, the wood samples were held at 105 °C, and the mass of samples was measured every 10 min using an analytical balance. Humidity 50% was the average humidity of samples prepared from fresh wood, so it was decided that the tests should be carried out on samples with such humidity. In the tests, care was taken to ensure that the prepared samples had such humidity, so that drying for different experiments could be compared in the entire range of humidity characteristic for wood. The target moisture content was achieved by soaking the samples in water.

Similarly, samples of pieces of wood with smaller dimensions of 20×20×5 mm were prepared. During this experimental analysis, the mass loss of the samples was determined within two-minute time periods for the fibres oriented along and across the heat source.

Pyrolysis process

Pyrolysis processes were conducted in a high-temperature batch reactor with an inert gas. The wooden samples were placed inside a hot furnace (the temperature of the process reached 500 °C) that was purged with an inert gas for the same time and temperature for each sample through the pyrolysis process. The simple construction of the pyrolysis reactor and the high thermal inertia allowed a partial pyrolysis of the sample to occur. The sample was removed from the furnace and cooled in a hermetic aluminium autoclave to stop the decomposition processes.

The samples with a size of 20×20×5 mm (AC and AL) were placed directly in the middle of the furnace, where convection was forced by conduction between one side of the sample and the furnace. The samples were heated in a furnace for 30, 60, 90, 120 and 150 s and weighed to determine the mass loss and degree of decomposition. This method has disadvantages, such as direct heating from the base of furnace or convection heating from the different sides. Five walls are heated in the furnace, the side walls and the top. To eliminate these problems, larger samples and vermiculite insulation were used in the other experiments. The non-insulated side (wall) of the samples with a size of 32×30×30 mm was subjected to the heat directly for 5, 10, 15, 20, 25 and 30 min. This forced convection in the non-insulated direction depended on the arrangement of the fibres (IAC and IAL) in the analysed samples.

The mass loss measurements were taken every 30 s, and the dynamics of the processes were presented as a per cent of the mass loss in 1-min intervals to unify all

experiments in this work. The samples after pyrolysis were analysed using the radiographic method.

Radiographic testing (X-ray image analysis)

Radiographic testing (RT) was conducted using a low-power X-ray tube at a voltage of 44 kV and current of 10 mA. The analysis relies on irradiating a sample with a radiation source using an X-ray tube or a radioactive isotope, and the irradiated object emits ionizing radiation. The emitted radiation is applied to a radiographic film or an image plate (in the case of digital radiography). In this study, phosphor imaging plates were used during computed radiography (CR) to obtain a digital image. This type of radiography has many advantages compared to traditional radiography, such as the ability to display sharp images and enlarge specific areas.

Mathematical model of pyrolysis process

Simultaneously with the experimental work, a mathematical model of the pyrolysis of a single wooden particle was developed, and calculations using mass loss and temperature distribution were performed. The calculations were performed for the smaller, non-insulated sample (Fig. 1A, C) in order to put an emphasis on the influence on fibre orientation on the heat transfer processes and as a result on the pyrolysis process.

The effect of wooden fibre orientation was previously studied by Gronli (1996). The author conducted a thorough study, distinguishing three alternately arranged layers of wooden matter: substance/fibres, bound/liquid water, and gas. Gronli calculated the value of thermal conduction coefficient for parallel and perpendicular fibre orientation (in this work: along and across, respectively) for various moisture content. Based on these results, values of thermal conductivity for two fibre orientations of dry wood were implemented in this model (Table 1).

Table 1 Physico-chemical parameters of the wooden sample implemented in the computational model

Material	Parameter	Value	Reference
Wood	$\rho_w, \frac{kg}{m^3}$	660	Own analysis
Char	$\rho_c, \frac{kg}{m^3}$	204	Own analysis
Wood	$c_{p,w}, \frac{J}{kgK}$	$1500 + T$	Gronli (1996)
Char	$c_{p,c}, \frac{J}{kgK}$	$420 + 2.09T\text{-}6.85\cdot10^{-4}T^2$	Gronli (1996)
Wood, along	$\lambda_w, \frac{W}{mK}$	0.38	Gronli (1996)
Wood, across		0.15	
Char	$\lambda_c, \frac{W}{mK}$	$0.0002T\text{-}0.0183$	Park et al. (2016)
Wood, char	$k, \frac{1}{s}$	$2.45 \cdot 10^5 \cdot \exp\left(-\frac{95.4}{RT}\right)$	Gronli (1996)

The prepared model is one-dimensional, transient. To simplify the model it was assumed that the heat was being provided through the top and bottom wall only. Thermal parameters and mass loss were calculated with the direction of heat input (Fig. 3). The simulated sample was implemented to be 5 mm long in total, divided into 200 cells. Initial temperature of the whole sample was set to 20 °C. Similarly to the experimental work, the sample was subjected to the immediate temperature of the surroundings; therefore, the boundary condition was set to 500 °C for walls of the sample.

The approach focuses on a solution of a two-equation system involving mass loss and heat transfer equation in the following form:

$$\frac{\partial \alpha}{\partial t} = -k\left(\alpha - \overline{\alpha}\right),$$

where: t is time, α is a mass ratio of current mass (solid) to initial mass of the sample (m_s/m_0) and $\overline{\alpha}$ is ratio of mass loss function obtained for pyrolysis process with a very slow heating rate to the initial mass of the sample ($\overline{m}/m_0$).

The reason of including the additional parameter $\overline{\alpha}$ is described thoroughly in previous works (Kardaś et al. 2019; Postrzednik 1994). In the above equation k is a chemical reaction rate coefficient.

The heat transfer equation is considered in the following form:
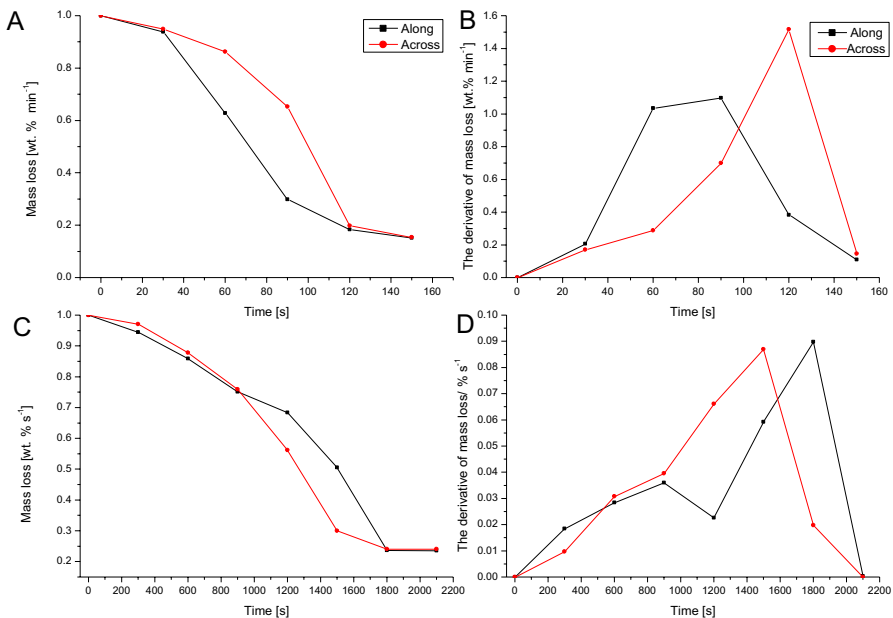
Fig. 3 The pyrolysis process dynamic for particles with fibres oriented across and along the heat source: **A** and **B**. 20×20×5 mm samples (not insulated) and **C** and **D**. 32×30×30 mm samples (insulated on 5 walls)

$$\frac{\partial T}{\partial t} = \frac{\lambda}{\varrho c_p} \frac{\partial^2 T}{\partial z^2},$$

where T is temperature, t is time, ρ is density of the sample, c_p is a specific heat capacity, and λ is thermal conductivity.

The physical parameters are functions of temperature and/or the pyrolysis process stage (α). All the implemented values are gathered in Table 1. The values of the parameters of the sample at a given temperature were based on the pyrolysis stage, as follows:

$$\lambda(T, \alpha) = \alpha(T) \cdot \lambda_w + (1 - \alpha) \cdot \lambda_c(T)$$

for thermal conductivity,

$$c_p(T, \alpha) = \alpha(T) \cdot c_{p,w}(T) + (1 - \alpha) \cdot c_{p,c}(T)$$

for specific heat capacity, and

$$\varrho(T, \alpha) = \alpha(T) \cdot \varrho_w + (1 - \alpha) \cdot \varrho_c$$

for density.

Results and discussion

Drying results

Figure 1 presents the rate of water mass loss (%) as a function of time (s) for the $20 \times 20 \times 5$ mm (not insulated) and $32 \times 30 \times 30$ mm samples, and the dynamics of the processes are expressed as weight loss in % (related to initial mass) in 1-min intervals.

The highest dynamic of the drying process for all the samples was observed at the beginning (first 300 s) of the process. This resulted from the removal of water on the surface of the tested material. In the subsequent stages of the drying process, the van der Waals-bound water in the pores of the biomass was removed. In comparison with the AC and AL samples, the IAC and IAL samples were characterized with a greater process dynamics variability that was influenced by the insulation of the walls and limitation of the heat exchange surface.

Despite the different physical properties, such as the thermal conductivity along a specific wall of the samples, the time of drying process was similar. Samples with fibres along the heat source (AL and IAL) were better heat conductors in terms of providing heat inside the sample. In this case, the direction of vapour flow (outflow) was away from the heat source. Therefore, the heat penetration was partially counterbalanced by the oppositely directed fluid flow (heat removal). In the case of samples with fibres oriented across the heat source (AC and IAC), the heat penetration was more difficult because of the alternatively arranged layers of high and low thermal conductivity materials (Fig. 2).

Pyrolysis results

In Fig. 3, the pyrolysis processes, mass loss of the samples in time and the dynamics of the processes expressed in per cent of the mass loss in time for the $20 \times 20 \times 5$ mm samples (not insulated) and $32 \times 30 \times 30$ mm samples (insulated on 5 walls) are presented. The orientation of the wood fibres in the first type of samples (not insulated) did not influence the mass loss for the first 30 s of the pyrolysis process (20% of the overall process time). In the second step after 40 s, the intensity of the decomposition was higher for the sample with fibres oriented along the heat source (AL). The maximum dynamics of the mass loss for the AL samples was in the 90th second of the process, and there was 70 wt. % of mass loss per minute. Degradation of the AC samples was slower than that for the AL samples, especially in the initial stage of the process. The dynamics increased at the final stage of the process and achieved a maximum of 90 wt. % of mass loss per minute, which significantly exceeded the maximum of that for the other samples. The end of the process was reached after 120 s and was the same for both types of fibre orientation (AC and AL). Despite the differences in the rate of the process, the decomposition took place at a similar time with similar final values.

The pyrolysis process of the insulated $30 \times 30 \times 32$ mm samples is presented in Fig. 3C-D. During the first 15 min of the process, the mass loss for both sample sizes was similar and the dynamics of process was low. The IAC samples had a slightly higher mass loss during the degradation process. In the next steps, the IAL samples rapidly decomposed, with a final mass that was 24 wt.% of the initial mass after 30 min of the process. The intensity of the volatilization increased from the beginning of the process up to 20 min, where it reached a maximum of 5.22 wt. % mass loss per minute. Volatilization of the IAC sample occurred with a different dynamic (like that for the smaller samples AC and AL). After 20 min of degradation, the process was slower than that for the IAL samples. Between the 10th and 20th minute, the pyrolysis slightly decreased and then the dynamic of the process increased again and reached its maximum at the 25th minute, with 5.39 wt.% of mass loss per minute. The pyrolysis of the IAC and IAL samples was slower than that for the AC and AL samples for most steps of the process. The dynamic increased at the end of the process, and for both fibre orientations, a similar final mass of 23.5 wt.% of the initial mass after 30 min resulted. Similar to the case of the uninsulated samples (AC and AL), the rate of the process was different, but the final effect was very similar (24 wt.% of the initial mass for IAL and 23.5 wt.% of the initial mass for IAC samples).
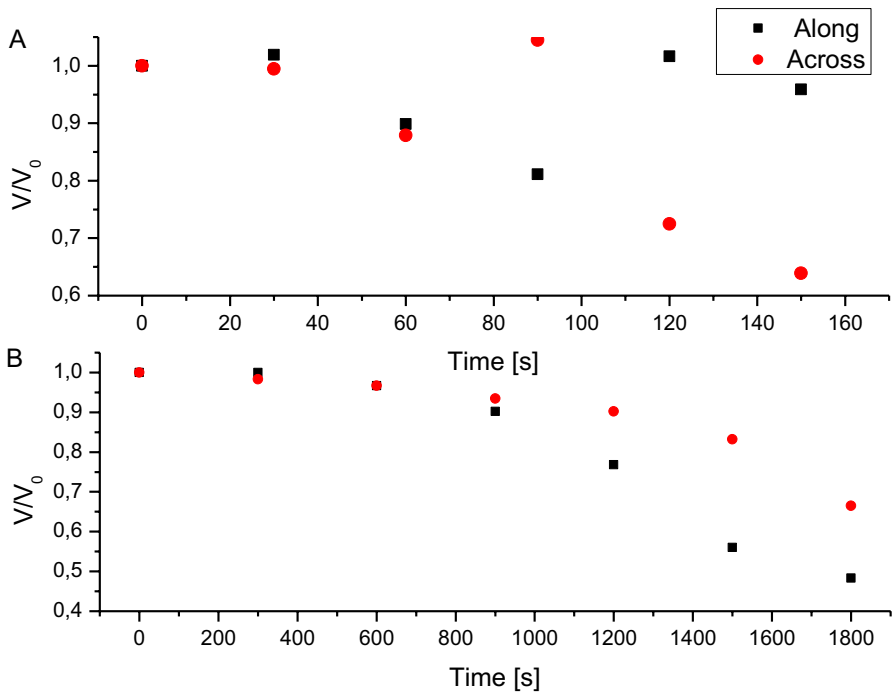
Volume change analysis

Volume change analysis was carried out in a simple manner. Measurements of each of the three dimensions of the cube (length, width, height) were made for two places, i.e., for the point at the corner and in the middle of the segment. After taking the average, this value was used to calculate the volume. Measurements

were taken with a caliper. This measurement, although simple, shows the direction of changes quite well.

The changes in the sample volumes were analysed in both series of experiments (two size samples and two types of fibre orientation), and the changes in volume are compared in Fig. 4.

The cuboid shape of the $20 \times 20 \times 5$ mm AL samples after pyrolysis curved into an arch. During decomposition, the volume of the AL and IAL samples changed significantly, which was the consequence of the generation of gases and deformation of the samples. The volume for the AL sample was 63% of the initial volume, while for the AC sample, the decrease was not noticeable (95% of the initial volume). A similar tendency was observed for the large samples (IAC and IAL), where a higher volume loss was obtained for the IAL samples (48% of the initial volume) than for the IAC samples (66% of the initial volume). It is worth noting that for samples welded along the fibres, the sample increases in volume at some point. The observed effect is the result of stress caused by deformation.

Fig. 4 Change in volume of the samples during the pyrolysis process: **A**. $20 \times 20 \times 5$ mm samples (not insulated) (AC and AL) and **B**. $32 \times 30 \times 30$ mm samples (insulated on 5 walls) (IAC and IAL)

X-ray image analysis

Analysis of the mass and volume changes of the AC, AL, IAC, and IAL wood samples during pyrolysis using traditional thermogravimetric analysis (TGA) provided similar results, and the differences were slight. A similar result is due to the low mass and volume of the samples used in the TGA. The parameter limiting the rate of pyrolysis is primarily the rate of heat supply to the samples. The aim of this study was to prove that the proposed innovative method, namely, radiography, enables the observation and analysis of sample conversion during the process. This method complements TGA and allows a better understanding of heat transfer processes during thermal degradation of samples.

The novelty of using X-ray images is that it allows one to observe the inside of the samples during the degradation process. The mass loss rate during pyrolysis was comparable during the first 15 min for both fibre orientations. One should be aware that regardless of whether the wood sample is pyrolysed or not, the photographs taken along the fibres will be characterized by greater contrasts in individual parts of the photograph. Trees grow by one annual ring each year. The annual ring is a layer consisting of early and late wood. Early wood formed in the spring is characterized by greater porosity and lower density. Wood formed in this period is used to transport water in the tree. Late wood performs mainly mechanical functions and has a high density and low porosity.

The deformation of samples AC and AL (not insulated) involved a shape change and volume decrease as the time of the process increased, as presented in the X-ray images in Fig. 5. The lower colour contrast represents a lower density; therefore, the density decreased as the process progressed.

The IAL samples were determined to have a weaker heat transfer to the inside of the particle compared with that for the IAC samples (Figs. 6 and 7). This resulted in strong carbonization of the outer layer of the sample with a low decomposition degree in the deeper layers of the wood. The X-ray images show a greater colour contrast for the IAC samples that involve a higher density differences and a strong distinction between the decomposed and undecomposed zones in the sample. The
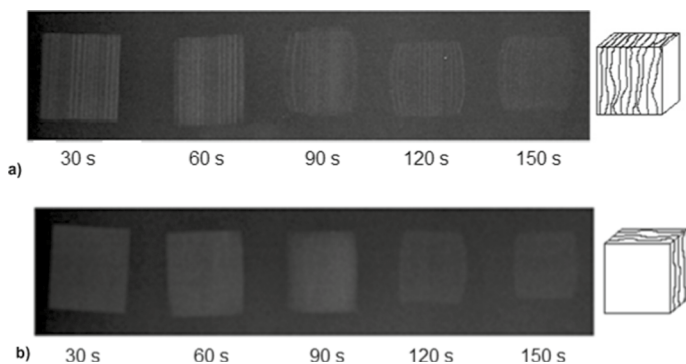
Fig. 5 X-ray images of flat $20\times20\times5$ cm samples: **a** AC and **b** AL
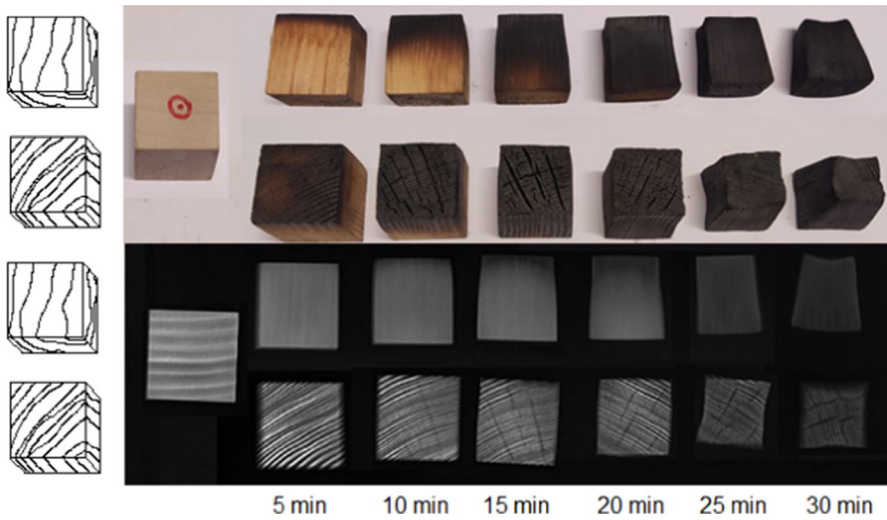
Fig. 6 X-ray and standard images of the wooden samples with fibres oriented along to the direction of the heat source
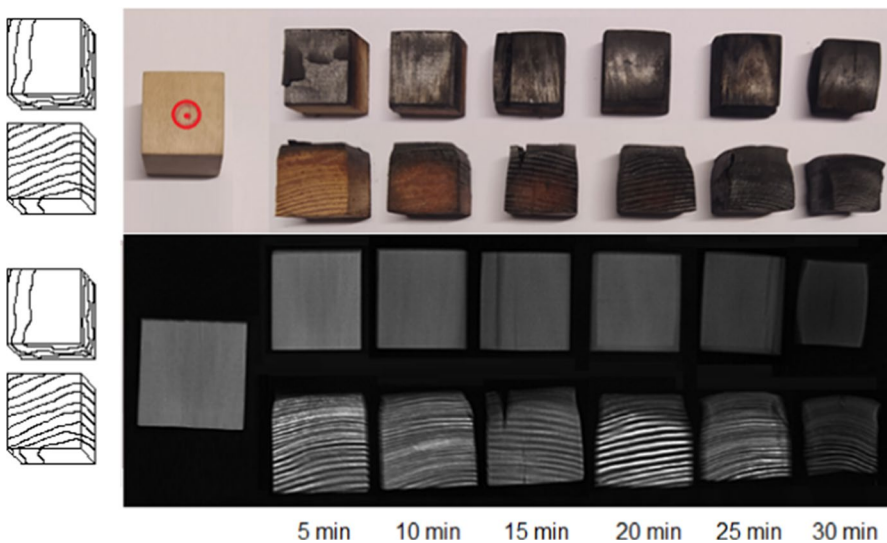
Fig. 7 X-ray and standard images of wooden samples with fibres oriented across with respect to heat source

faster heat transfer deeper into the particle for a larger volume of the IAL sample influenced the slightly carbonized region during the initial phase of the process. However, these were decomposition processes characteristic for lower temperatures (CO and CO_2 release occurred as well as evaporation of water). After 15 min, the dynamic changed for the AL and IAL samples because they decomposed more

dynamically due to several factors, such as more intensive gas conduction and heat transfer along the fibres and the appearance of cracks. Characteristic cracks in the wooden core appeared for both samples (AL and IAL) after 5 min of the process. The cracks were located with a 90 degrees angle with respect to the wood fibres (Fig. 6). In Fig. 6, the cracks for the samples at 10th, 15th and 20th minute were visible. The two last samples in Fig. 6 (IAL at the 25th and 30th minutes) did not have cracks, but the X-ray photographs indicated that the cracks were present. The cracks formed for all the samples from 10th minute and above, which could be observed without special equipment due to a change in the shapes of the samples (volume decrease).

The cracks in the AC and IAC samples were almost non-existent, and the regularity of their formation cannot be demonstrated. In this case, the dynamics of the process are presented in Fig. 4 and compared with the X-ray images. The AL and IAL samples were darker than the AC and IAC samples, which indicates a lower density. The sample decomposed dynamically only at the final stages of pyrolysis; this can be seen in the X-ray images, where there is a large difference in colour when comparing the two last samples in Fig. 7 (25th and 30th minutes). Due the low thermal conductivity for the samples with this fibre orientation, the flattening of the mass loss curve can be observed between the 15th and 20th minutes.

Theoretical and experimental mass loss curve for along and across wood sample

The results of calculation can be observed in Fig. 8. Results of mass loss presented in Fig. 8 are mostly used for the validation of the model. It can be seen that the mass loss (pyrolysis stage) progress is consistent with the experimental data. Intensity of the devolatilization processes is similar for the given temperature ranges. The final mass ratio of the simulated sample is of a similar value to the experimental samples. The total time of decomposition of the simulated process is in compliance with the measured values. This confirms that the calculation results are a valid representation of the experimental work.
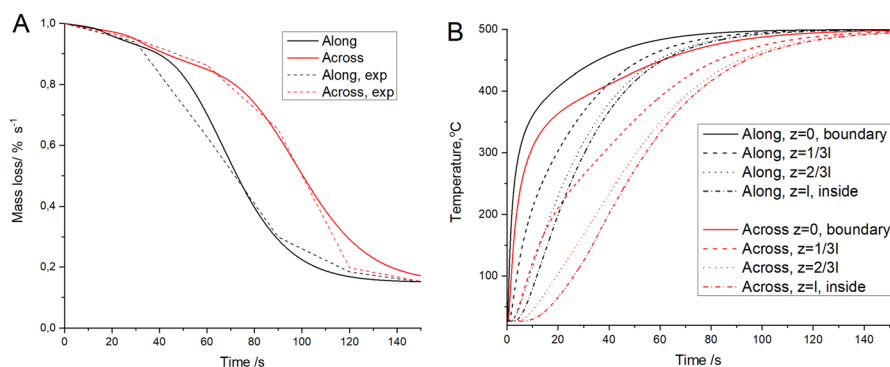
Fig. 8 Calculation results. **A:** Mass loss function in time (calculation results compared with experimental data); **B:** Temperature distribution along the samples
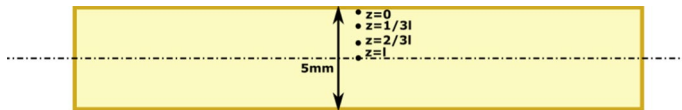
Fig. 9 Temperature points measured in Fig. 9. The value of l is half of the sample width, $l = 2{,}5$ mm

Figure 8B presents temperature distributions in time of the process for four points across the half of the sample (see schematic Fig. 9). In general, it can be observed that the further the point is from the edge of the sample, the lower the temperature in a given time. Moreover, it takes more time to reach the final temperature of 500 °C for locations further from the wall. This is a natural consequence of heat transfer process. However, the most important observation is during the comparison of the two sets of data in Fig. 8B: temperature distribution for sample with fibres oriented along (black dataset) and across (red dataset) the heat source. Thereby for a certain time the temperatures for sample with fibres across the heat source are lower. This means that the AC sample heats up slower than the AL sample. This effect is caused by the fibres oriented in a way that provides either higher (AL) or lower (AC) heat transfer rate. This in turn implies the decomposition process dynamics. Lower temperatures of the AC sample cause lower mass loss rate, and it takes more time to decompose the sample with fibres oriented across the heat source (Fig. 8A).

Conclusion

During the drying of the $20 \times 20 \times 5$ mm samples, the mass loss at the beginning of the process was much faster and dynamic for the fibres oriented along the direction of the heat source. After 50 s of pyrolysis, the mass difference between the not insulated samples ($20 \times 20 \times 5$ mm) was approximately 25 wt.%, and after 90 s, the difference increased to over 30 wt.%. Although the pyrolysis rate of both samples differed, the final mass was similar and amounted to approximately 18 wt. % of the initial mass. Despite these apparently similar results for samples AC and AL, the structure of the woody biomass had a significant impact on the mechanism and dynamics of pyrolysis process. Traditional TG provided similar results. However, a detailed analysis using the novel radiographic method allows one to observe different aspects of the process in addition to the deformation and change in the shape of the wood sample. The dynamics are closely related to the structure of the analysed samples and may have a significant impact on the properties of the obtained carbon material.

The obtained radiographic images were different depending on the degree of decomposition. During the decomposition process, the density of the sample decreased, which was observed through differences in the colour intensity and contrast on the image. The process did not take place with the same speed over the entire volume of the sample, which resulted in a reduction in the decomposition degree during slow heat transfer into the sample.

The presented numerical calculations allowed to demonstrate that the heat conduction is of fundamental role in the pyrolysis process. It was a proposal of a very simple model, consisting of two partial differential equations, and an attempt to check whether it can be successfully used for pyrolysis modelling in the case of larger samples. It seems that the answer is positive.

The presented research shows the wide possibilities of the radiographic technique in the study of pyrolysis. In addition to the analysis of pyrolysis dynamics, this technique gives the opportunity to observe sample defects resulting from stresses caused by temperature deformation of samples.

Declarations

References

Barr MR, Jervis R, Zhang Y, Bodey AJ, Rau C, Shearing PR, Brett DJL, Titirici M-M, Volpe R (2021) Towards a mechanistic understanding of particle shrinkage during biomass pyrolysis via synchrotron X-ray microtomography and in-situ radiography. Sci Reports 11:1–13. https://doi.org/10.1038/s41598-020-80228-x

Boigné E, Bennett NR, Wang A, Mohri K, Ihme M (2021) Simultaneous in-situ measurements of gas temperature and pyrolysis of biomass smoldering via X-ray computed tomography. Proc Combust Inst 38:3899–3907. https://doi.org/10.1016/J.PROCI.2020.06.070

Boigné E, Bennett NR, Wang A, Ihme M (2022) Structural analysis of biomass pyrolysis and oxidation using in-situ X-ray computed tomography. Combust Flame 235:111737. https://doi.org/10.1016/J.COMBUSTFLAME.2021.111737

de Jesus MS, de Carneiro ACO, Martinez CLM, Vital BR, Carneiro APS, de Assis MR (2019) Thermal decomposition fundamentals in large-diameter wooden logs during slow pyrolysis. Wood Sci Technol 53:1353–1372. https://doi.org/10.1007/S00226-019-01133-9/TABLES/4

Demirbaş A (2001) Carbonization ranking of selected biomass for charcoal, liquid and gaseous products. Energy Convers Manag 42:1229–1238. https://doi.org/10.1016/S0196-8904(00)00110-2

Forest Service U, Products Laboratory F (2020) Wood Handbook, Wood as an Engineering Material, 2010. www.fpl.fs.fed.us. Accessed August 19, 2020

Grønli MG (1996) A theoretical and experimental study of the thermal degradation of biomass, The Norvegian University of Science and Technology

Guo W, Lim CJ, Bi X, Sokhansanj S, Melin S (2013) Determination of effective thermal conductivity and specific heat capacity of wood pellets. Fuel. https://doi.org/10.1016/j.fuel.2012.08.037

Haboub A, Bale HA, Nasiatka JR, Cox BN, Marshall DB, Ritchie RO, Macdowell AA (2014) Tensile testing of materials at high temperatures above 1700 °C with in situ synchrotron X-ray micro-tomography. Rev Sci Instrum 85:083702. https://doi.org/10.1063/1.4892437

Januszewicz K, Kazimierski P, Klein M, Kardaś D, Łuczak J (2020) Activated carbon produced by pyrolysis of waste wood and straw for potential wastewater adsorption. Materials 13:2047. https://doi.org/10.3390/ma13092047

Jones K, Ramakrishnan G, Uchiyma M, Orlov A (2015) New applications of X-ray tomography in pyrolysis of biomass: biochar imaging. Energy Fuels 29:1628–1634. https://doi.org/10.1021/EF5027604/SUPPL_FILE/EF5027604_SI_001.PDF

Kardaś D, Hercel P, Polesek-Karczewska S, Wardach-Święcicka I (2019) A novel insight into biomass pyrolysis—the process analysis by identifying timescales of heat diffusion, heating rate and reaction rate. Energy. https://doi.org/10.1016/j.energy.2019.116159

Kardaś D, Kluska J, Klein M, Kazimierski P, Heda Ł (2014a) Modelowe kompleksy agroenergetyczne: Teoretyczne i eksperymentalne aspekty pirolizy drewna i odpadów (Model agroenergy complexes: Theoretical and experimental aspects of wood and waste pyrolysis.), Wydawnictwo UWM, Olsztyn

Kardaś D, Turzyński T, Wardach-Święcicka I, Ronewicz K (2014b) Spalanie i wymiana ciepła w olejowym kotle na biomasę (Combustion and heat exchange in an oil-fired biomass boiler.), Wydawnictwo IMP PAN

Kazimierski P, Vieira S, Kardaś D (2020) Pine wood particles pyrolysis and radiographic analysis. Drv Ind 71:13–18. https://doi.org/10.5552/DRVIND.2020.1834

Kazimierski P, Hercel P, Suchocki T, Smoliński J, Pladzyk A, Kardaś D, Łuczak J, Januszewicz K (2021) Pyrolysis of pruning residues from various types of orchards and pretreatment for energetic use of biochar. Mater. 14:2969. https://doi.org/10.3390/MA14112969

Kazimierski P, Januszewicz K, Godlewski W, Fijuk A, Suchocki T, Chaja P, Barczak B, Kardaś D (2022) The course and the effects of agricultural biomass pyrolysis in the production of high-calorific biochar. Mater 15:1038. https://doi.org/10.3390/MA15031038

Kluska J, Ronewicz K, Kardaś D (2019) Characteristics of single wood particle pyrolysis using particle image velocimetry. Int J Therm Sci 135:276–284. https://doi.org/10.1016/j.ijthermalsci.2018.09.020

Kollmann FFP, Côté WA (1968) Principles of wood science and technology, Springer Berlin Heidelberg. https://doi.org/10.1007/978-3-642-87928-9

Mathews JP, Campbell QP, Xu H, Halleck P (2017) A review of the application of X-ray computed tomography to the study of coal. Fuel 209:10–24. https://doi.org/10.1016/J.FUEL.2017.07.079

Murai K, Daitoku T, Tsuruda T (2021) Three-dimensional analysis of the pyrolysis behavior of solid fuel by ultra high-speed X-ray CT. Proc Combust Inst 38:3987–3994. https://doi.org/10.1016/J.PROCI.2020.08.026

Park JS, Lee JJ (2016) Fire resistance of light-framed wood floors exposed to real and standard fire. J Fire Sci 22:449–471. https://doi.org/10.1177/0734904104042548

Postrzednik S (2022) Heat of solid fuel pyrolysis-determination method, basic properties, in Polish, in: Karbo-Energochemia-Ekologia, 1994. https://scholar.google.com/scholar_lookup?title=Heat of solid fuel pyrolysis - determination method%2C basic properties&publication_year=1994&author=S. Postrzednik. Accessed November 15, 2022

Ronewicz K (2017) Piroliza cząstki biomasy w strumieniu gorących gazów (Pyrolysis of biomass particles in a stream of hot gases.), IMP PAN

Siau J (1984) Transport processes in wood, Springer-Verlag, Berlin

Suleiman BM, Larfeldt J, Leckner B, Gustavssor M (1999) Thermal conductivity and diffusivity of wood. Wood Sci Technol 33:465–473. https://doi.org/10.1007/S002260050130/METRICS

Wardach-Święcicka I, Kardaś D (2013) Modeling of heat and mass transfer during thermal decomposition of a single solid fuel particle. Arch Thermodyn 34:53–71. https://doi.org/10.2478/aoter-2013-0010

Yin F, Du Y, Li Z, Jiang J (2023) Water vapor sorption characteristics and hysteresis of earlywood and latewood within the same growth ring of *Catalpa bungei*. Wood Sci Technol 57:507–521. https://doi.org/10.1007/S00226-023-01457-7/METRICS